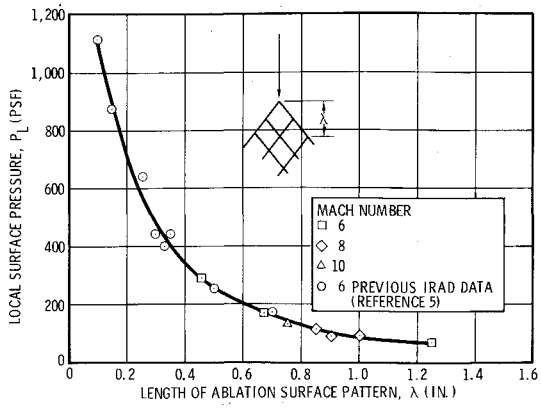

Fig. 3 Variation of camphor ablation surface pattern length with local surface pressure.

run, but was visible in the photographs and movies taken during the tests. The following results and conclusions are all based on the camphor data.

Results and Discussion

A 10° camphor cone after 43 sec at Mach 6 is shown in Fig. 1. This figure also shows the typical model construction with the sharp steel nose separated from the ablative material by a ceramic insulating spacer.

Pattern angle and size

One of the important objectives of these tests was to determine whether the pattern angle continues to lie close to the Mach angle as Mach number increases. Figure 2 shows the range of pattern angles obtained as a function of edge Mach number together with previous data. Figure 2 shows that the pattern angle continues to lie just above the edge Mach angle as Mach number increases.

Figure 3 shows the variation of the streamwise length of the ablation patterns with local surface pressure. Data from the previous in-house work at Mach 6 are included. It should be noted that the addition of higher Mach numbers and smaller cone angles did not invalidate the previous correlation, but merely extended it to higher pattern lengths and lower pressures. It can be shown that these data are consistent with the pattern angle vs Mach angle correlation of Fig. 2 and with the Probstein-Gold idea[7] that cross-hatching occurs because of a resonance between boundary-layer disturbance and a suitable inelastic deformable surface.

Effect of nosetip bluntness

To check the effect of nosetip blunting on cross-hatching, the 10° cone was tested with various radius nosetips. Figure 4 shows the pattern angles plotted vs their local edge Mach number. Data for the sharp nose as well as bluntness ratios of 0.05 and 0.15 are included. Even this moderate bluntness can reduce edge Mach number by nearly half and consequently has a marked influence on the pattern angle correlation. These data, which are plotted at the correct local edge Mach number, fit the sharp cone pattern angle versus edge Mach number correlation. If uncorrected, the 0.15 bluntness data would violate the correlation. There is no indication of a limiting minimum angle above Mach 3 as suggested by the flight data of Ref. 3 which are indicated in Fig. 3. It is believed that nose bluntness effects, such as those shown in Fig. 4, may resolve this discrepancy between flight and ground test data.

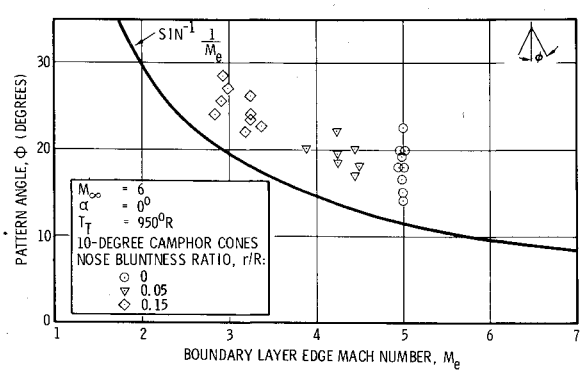

Fig. 4 Effect of nosetip bluntness on surface pattern angle.

Summary and Conclusions

Hypersonic wind-tunnel tests of conical camphor models extended the cross-hatching angle vs edge Mach number correlation, showed nosetip bluntness effects compatible with this correlation, and extended the curve showing pattern wavelength varying inversely with local pressure.

References

[1] Larson, H. K. and Mateer, G. G., "Cross-Hatching—A Coupling of Gas Dynamics with the Ablation Process," AIAA Paper 68-670, Los Angeles, June 1968.

[2] Canning, T. N., Wilkins, M. E., and Tauber, M. E., "Ablation Patterns on Cones Having Laminar and Turbulent Flows," *AIAA Journal*, Vol. 6, No. 1, Jan., 1968, pp. 174–175.

[3] Laganelli, A. L. and Nestler, D. E., "Surface Ablation Patterns: A Phenomenology Study," *AIAA Journal*, Vol. 7, No. 7, July 1969, pp. 1319–1325.

[4] Nachtsheim, P. R. and Larson, H. W., "Cross-hatched Ablation Patterns in Teflon," *AIAA Journal*, Vol. 9, No. 8, Aug. 1971, pp. 1602–1607.

[5] Williams, E. P., "Experimental Studies of Ablation Surface Patterns and Resulting Roll Torques," *AIAA Journal*, Vol. 9, No. 7, July 1971, pp. 1315–1321.

[6] Williams, E. P. Inger, G. R., "Investigations of Ablation Surface Cross-Hatching," SAMSO TR70-246, June 1970, USAF Space and Missile Systems Organization, Norton Air Force Base, Calif.

[7] Gold, H., Probstein, R. J., and Scullen, R. S., "Inelastic Deformation and Crosshatching," AIAA Paper 70-768, Los Angeles, June 1970.

Quasi-Static Thermal Stresses due to a Moving Heat Source in a Circular Disk

THOMAS J. KIM*
University of Rhode Island, Kingston, R. I.

Nomenclature

a = radius of disk or cylinder
E = Young's modulus
h = heat-transfer coefficient
k = thermal conductivity
r_o = radial coordinate of heat source
T = temperature
Q_o = intensity of heat source
α = thermal expansion coefficient
β = h/k
κ = thermal diffusivity
λ_m = eigenvalues
ν = Poisson's ratio
ξ = phase angle
ϕ = stress function
ω = angular velocity
∇^2 = Laplacian operator

Received April 22, 1971.

* Assistant Professor of Mechanical Engineering and Applied Mechanics.

Introduction

IN this Note a closed form solution is obtained for a stress field generated by a moving point heat source in a circular disk of radius a (or a line heat source in a long solid circular cylinder). The theory of two-dimensional uncoupled quasi-static thermoelasticity is used.[1] The disk or cylinder is assumed to be made of isotropic homogeneous material. The planes bounding the disk are thermally insulated and the radial surface is subjected to the heat exchange with the surrounding fluid medium. It is believed that the result obtained from the present analysis would be of considerable practical importance in welding problems.

Analysis

The equation governing the two-dimensional thermal problems may be expressed in terms of the stress function $\phi(r,\theta,t)$ which satisfies

$$\nabla^4\phi + \bar{m}\nabla^2 T = 0 \tag{1}$$

where $\bar{m} = \alpha E$ for plane state of stress and $\bar{m} = \alpha E/(1-\nu)$ for plane state of strain. The stresses in the plane state of stress have the form

$$\sigma_r = (1/r^2)(\partial^2\phi/\partial\theta^2) + (1/r)(\partial\phi/\partial r)$$
$$\sigma_\theta = \partial^2\phi/\partial r^2 \qquad \zeta_{r\theta} = -(\partial/\partial r)[(1/r)(\partial\phi/\partial\theta)] \tag{2}$$

Temperature field

For a moving heat source of constant intensity Q_o which is rotating along a circular path $r = r_o$ with a constant angular velocity ω, the temperature field satisfies the heat conduction equation

$$\nabla^2 T = \frac{1}{\kappa}\frac{\partial T}{\partial t} - \frac{Q_o}{\kappa}\frac{\delta(r-r_o)\delta(\theta-\omega t)}{r} \tag{3}$$
$$0 < r \leq a \qquad 0 < t \leq \frac{2\pi}{\omega}$$

where $\delta(r)$ and $\delta(\theta)$ are Dirac's Delta functions. The initial and boundary conditions are

$$T(r,\theta,0) = 0$$
and
$$\partial T/\partial r = -\beta T \quad \text{at } r = a \tag{4}$$

in which the temperature of surrounding medium is assumed to be zero. Since the heat source term in Eq. (3) may be expanded in the form of

$$\frac{Q_o}{\kappa\pi}\sum_{m=1}^{\infty}\sum_{n=0}^{\infty} D_{mn}J_n(\lambda_m r)\cos n(\theta-\omega t) \tag{5}$$

where

$$D_{mn} = \frac{2\lambda_m^2 J_n(\lambda_m r_o)}{(\lambda_m^2 a^2 - n^2)J_n(\lambda_m a) + a^2\lambda_m^2[J_n'(\lambda_m a)]^2} \tag{6}$$

the complete solution to Eq. (3) can be assumed as

$$T(r,\theta,t) = \sum_{m=1}^{\infty}\sum_{n=0}^{\infty} J_n(\lambda_m r)[A_{mn}(t)\cos n\theta + B_{mn}(t)\sin n\theta] \tag{7}$$

where λ_m are the positive roots of

$$\lambda_m J_n'(\lambda_m a) + \beta J_n(\lambda_m a) = 0 \tag{8}$$

Substituting Eq. (7) into Eqs. (3) and (4), one can obtain a system of differential equations for A_{mr} and B_{mn}, and it is

$$(\dot{A}_{mn},\dot{B}_{mn}) + \kappa\lambda_m^2(A_{mn},B_{mn}) = \frac{Q_o D_{mn}}{\pi}(\cos n\omega t, \sin n\omega t) \tag{9}$$

and

$$\dot{A}_{mn}(0) = \dot{B}_{mn}(0) = 0$$

The solutions obtained from Eq. (9) and assumed T in Eq. (7) yield

$$T = \frac{2Q_o}{\kappa\pi}\sum_{m=1}^{\infty}\sum_{n=0}^{\infty} T_{mn}J_n(\lambda_m r)[(\cos n\theta + d_{mn}\sin n\theta)e^{-\kappa\lambda_m^2 t} - d_{mn}\sin n(\theta-\omega t) + \cos n(\theta-\omega t)] \tag{10}$$

where

$$T_{mn} = \frac{J_n(\lambda_m r_o)}{(\lambda_m^2 a^2 - n^2 + a^2\beta^2)J_n^2(\lambda_m a)(1+d_{mn}^2)}$$

and

$$d_{mn} = n\omega/\kappa\lambda_m^2$$

Stress field

The stress function ϕ may be decomposed as

$$\phi(r,\theta,t) = \phi_1(r,\theta,t) + \phi_2(r,\theta,t) \tag{11}$$

which reduces Eq. (1) to the system of equations

$$\nabla^4\phi_1 = 0 \tag{12}$$

and

$$\nabla^2\phi_2 = -\bar{m}T \tag{13}$$

The particular solution of Eq. (13) is easily obtained as

$$\phi_2 = \frac{2Q_o\bar{m}}{\kappa\pi}\sum_{m=1}^{\infty}\sum_{n=0}^{\infty}\frac{T_{mn}J_n(\lambda_m r)}{\lambda_m^2}\times [(-\cos n\theta + d_{mn}\sin n\theta)e^{-\kappa\lambda_m^2 t} - d_m\sin n(\theta-\omega t) + \cos n(\theta-\omega t)] \tag{14}$$

The solution of the biharmonic Eqs. (12)[2] may be assumed to take the form of

$$\phi_1 = b_o r^2 + \sum_{n=1}^{\infty}[(a_n r^n + b_n r^{n+2})\cos n\theta + (c_n r^n \times d_n r^{n+2})\sin n\theta] \tag{15}$$

where b_o, a_n, b_n, c_n, and d_n are time dependent constants, and they are determined from the traction free boundary conditions

$$\phi = \partial\phi/\partial r = 0 \qquad \text{at } r = a \tag{16}$$

Hence, the stress function $\phi(r,\theta,t)$ is given by

$$\phi = \frac{Q_o\bar{m}}{2\kappa\pi}\left\{\frac{r^2}{2a}\sum_{m=1}^{\infty}\lambda_m J_o'(\lambda_m a)T_{mo}(1-e^{-\kappa\lambda_m^2 t}) + \sum_{m=1}^{\infty}\sum_{n=1}^{\infty}\frac{J_n(\lambda_m r_o)}{\lambda_m^2(\lambda_m a^2 - n^2 + a^2\beta^2)J_n^2(\lambda_m a)(1+d_{mn}^2)^{1/2}}\times\left[\frac{\{r^n(r^2-a^2)(n+a\beta) - 2a^2\}}{a^{n+2}}J_n(\lambda_m a) + 2J_n(\lambda_m r)\right]\times\left[\cos(n\theta-\xi)e^{-\kappa\lambda_m^2 t} - \sin n\theta\sin(\omega t-\xi) - \cos n\theta\cos(\omega t-\xi)\right]\right\}$$

where

$$\xi = \tan^{-1}(n\omega/\kappa\lambda_m^2)$$

and the stress components may be calculated from Eq. (2).

References

[1] Nowacki, W., *Thermoelasticity*, Addison-Wesley, Reading, Mass., 1962, p. 389.

[2] Timoshenko, S. P. and Goodier, J. N., *Theory of Elasticity*, 3rd ed., McGraw-Hill, New York, 1970, p. 132.